Validation of SAGE III/ISS solar water vapor data with correlative satellite and balloon-borne measurements

S.M. Davis[1], R. Damadeo[2], D. Flittner[2], K. H. Rosenlof[1], M. Park[3], W.J. Randel[3], E.G. Hall[4,5], D. Huber[2,6], D.F. Hurst[4,5], A.F. Jordan[4,5], S. Kizer[2,6], L.F. Millan[7], H. Selkirk[8,9], G. Taha[8,9], K. A. Walker[10], H. Vömel[11]

[1] NOAA Chemical Sciences Laboratory, Boulder, CO, USA

[2] NASA Langley Research Center, Hampton, VA, USA

[3] National Center for Atmospheric Research Atmospheric Chemistry Observations and Modeling Laboratory, Boulder, CO, USA

[4] NOAA Global Monitoring Laboratory, Boulder, CO, USA

[5] Cooperative Institute for Research in Environmental Sciences, University of Colorado at Boulder, Boulder, CO, USA

[6] Science Systems and Applications, Inc., Hampton, VA, USA

[7] Jet Propulsion Laboratory, California Institute of Technology, Pasadena, CA, USA

[8] NASA Goddard Space Flight Center, Greenbelt, MD, USA

[9] Universities Space Research Association, Greenbelt, MD, USA

[10] University of Toronto, Department of Physics, Toronto, ON, Canada

[11] National Center for Atmospheric Research Earth Observing Laboratory, Boulder, CO, USA

Corresponding author: Sean M. Davis (sean.m.davis@noaa.gov)

Key Points:

- Water vapor data from the Stratospheric Aerosol and Gas Experiment on the International Space Station are assessed
- Data screening procedures are described for removing anomalous data and data impacted by cloud interference
- With appropriate filtering, the new data agree with other correlative measurements within ~ 10% in the stratosphere

Abstract

Since June 2017, the Stratospheric Aerosol and Gas Experiment III instrument on the International Space Station (SAGE III/ISS) has been providing vertical profiles of upper tropospheric to stratospheric water vapor (WV) retrieved from solar occultation transmission measurements. The goal of this paper is to evaluate the publicly released SAGE III/ISS beta version 5.1 WV retrieval through intercomparison with independent satellite- and balloon-based measurements, and to present recommendations for SAGE III/ISS data quality screening criteria. Overall, we find that SAGE III/ISS provides high quality water vapor measurements. Low quality profiles are predominately due to retrieval instabilities in the upper stratosphere that cause step-like changes in the profile, and aerosol/cloud-related interferences (below ~20 km). Above 35 km, the retrieved uncertainty and noise in the data rapidly grow with increasing altitude due to relatively low extinction signal from water vapor. Below the tropopause, retrieved uncertainty increases with decreasing altitude due to enhanced molecular scattering and aerosol extinction. After screening low-quality data using the procedures described herein, SAGE III/ISS WV is shown to be in good agreement with independent satellite and balloon-based measurements. From 20 – 40 km, SAGE III/ISS WV v5.1 data exhibit a bias of 0.0 to -0.5 ppmv (~10 %) relative to the independent data, depending on the instrument and altitude. Despite its status as a beta version, the level of SAGE III/ISS WV agreement with independent data is similar to previous SAGE instruments, and therefore the data are suitable for scientific studies of stratospheric water vapor.

Plain Language Summary

Measurements of water vapor in the stratosphere are important for understanding climate change. This paper presents new measurements of stratospheric water vapor from an instrument aboard the International Space Station, and we describe methods for filtering the data to retain only the highest quality profiles for scientific analysis. The new measurements compare well to existing satellite and scientific balloon measurements of stratospheric water vapor, and therefore will be of use for studying year-to-year and longer-term changes in stratospheric water vapor.

1 Introduction

Water vapor plays an important role in determining the radiative balance of Earth's atmosphere, and variations in stratospheric water vapor (SWV) concentrations have been shown to affect radiative forcing (Forster & Shine, 1999; Solomon et al., 2010), ozone concentrations (Dvortsov & Solomon, 2001), and atmospheric circulation (Maycock et al., 2013). These variations in SWV can occur on sub-seasonal to decadal timescales, so accurate and continuous global measurements of SWV are essential in order to understand SWV variability over the range of relevant timescales. Although no formal satellite-based monitoring program exists for SWV, a number of temporally overlapping satellite instruments have been making measurements of SWV continuously since the launch of the Stratospheric Aerosol and Gas Experiment II (SAGE II) in 1984. This collection of satellite SWV measurements, which is described comprehensively by the second SPARC (Stratosphere-troposphere Processes And their Role in Climate) water vapor assessment (WAVAS-II, Lossow et al., 2019), includes both the SAGE II instrument (1984 – 2005, Damadeo et al., 2013), as well as the SAGE III instrument that flew aboard the METEOR-3M satellite (SAGE III/M3M, 2002 – 2005, Thomason et al., 2010).

In June 2017, a new SAGE III instrument aboard the International Space Station (SAGE III/ISS) began regular operation and has been making ~30 solar occultation measurements per day since that time. From these sunrise and sunset transmittance measurements, vertical profiles of ozone (Wang et al., 2020), nitrogen dioxide, water vapor, and aerosol extinction at multiple wavelengths are retrieved, and have been made publicly available as version 5.1.

2 SAGE III/ISS solar water vapor data

2.1 Instrument description and retrieval

The SAGE III/ISS instrument is essentially the same as the SAGE III/M3M instrument (W. Chu et al., 1997; W. P. Chu & Veiga, 1998) only with some additional hardware to operate onboard the International Space Station and an improved neutral density filter to eliminate thick plate etalon features in the solar events (Cisewski et al., 2014; Thomason et al., 2010). Like previous SAGE instruments, it uses the technique of solar occultation to produce line-of-sight (LOS) transmission profiles at each wavelength from the top of the atmosphere down to the cloud top (W. P. Chu & Mccormick, 1979). SAGE III/ISS is also capable of making observations using lunar occultation or limb scatter modes, but those measurements do not produce water vapor as a retrieval product and are thus not discussed here. As a CCD spectrometer, observations of absorption by water vapor in the atmosphere are made using 27 different pixel columns on the CCD between 933 nm and 958 nm, each with a spectral resolution of ~1 nm. Two additional pixel columns with similar resolution near 920 nm and 971 nm are also used. Collectively, this spectral range measures in the rho-sigma-tau bands in the water vapor spectrum as well as the Wulf band in the ozone spectrum.

This paper discusses the results of the version 5.1 beta release of water vapor. The retrieval algorithm is a non-linear Levenberg Marquardt, onion-peeling algorithm making use of the Curtis-Godson approximation forward model to turn wavelength-dependent LOS transmission profiles into profiles of water vapor, ozone, and aerosol simultaneously. Contributions from Rayleigh/molecular scattering are removed first, but ozone is not simply cleared out as an interfering species despite having an arguably more robust solution (of ozone extinction) from another part of the SAGE III/ISS retrieval algorithm (e.g., see Wang et al. (2020) for a description of the SAGE III/ISS ozone product). This is because doing so would make the water vapor solution dependent upon the relative accuracy of the ozone cross-section database used here (Bogumil et al., 2003) between the primary ozone solution spectral range (~600 nm) and that used for water vapor (~945 nm). Similar retrievals in SAGE II using the same cross-section database suggest that the relative difference in ozone cross-sections between the two spectral regimes could be off by about 10% (Damadeo et al., 2013). Instead, the increased spectral resolution of SAGE III/ISS (compared to SAGE II) makes the retrieval sensitive only to the relative shape of the ozone cross-sections in the water vapor channel and not their overall magnitude (Thomason et al., 2010). However, the ozone and aerosol solutions that derive from the water vapor retrieval are not reported as part of the public data product. It is important to point out that in v5.1, unlike other SAGE III/ISS data products, the water vapor retrieval is performed on a 1 km grid and the results are interpolated to a 0.5 km grid. The LOS transmission profiles are also smoothed for use with the water vapor retrieval, giving the final product a 2 km vertical resolution.

The SAGE III/ISS instrument and its operation in solar occultation mode is similar to its predecessors (e.g., SAGE II and SAGE III/M3M), but includes some advances which permit measurement of additional wavelengths. A general description of the solar occultation measurement technique is provided by Mccormick et al. (1979), but here we briefly describe how SAGE III/ISS acquires the radiant target and uses a scanning mirror to scan the target image across the instrument field-of-view (FOV) aperture. A measurement is considered to occur at the point along the line of sight from the instrument to the target that comes closest to the Earth's surface (i.e., the subtangent point). The altitude of that point above the Earth's surface is commonly referred to as the tangent altitude.

The use of a scanning mirror provides multiple samples at each tangent altitude that are combined to construct transmission profiles from the Earth's surface (or cloud top) to an altitude of 100 km. Above this altitude, irradiance measurements are acquired between 100 and 250 km to characterize the instrument's performance across its wavelength range. This information is used to calibrate the instrument for each solar occultation event. By using this procedure, SAGE III data are relatively unaffected by changes in the instrument characteristics over the lifetime of the mission.

2.2 SAGE III/ISS solar sampling characteristics

The ISS is inclined in a 52° orbit, and as such, sunrise and sunset latitudes oscillate from their extreme latitude in one hemisphere to their extreme in the other hemisphere approximately every 30 days (Figure 1a). This pattern results in expanded sampling coverage compared to SAGE III/M3M. The latitudinal sampling envelope varies seasonally, in phase with the subsolar latitude, such that the sampling is shifted northward during boreal summer and southward during boreal winter. As with other mid- and high-inclination orbit solar occultation instruments, the sampling is denser at higher latitudes and sparser in the tropics, with on average 2-3 months per year of no tropical data at near-equatorial latitudes (Figure 1b).

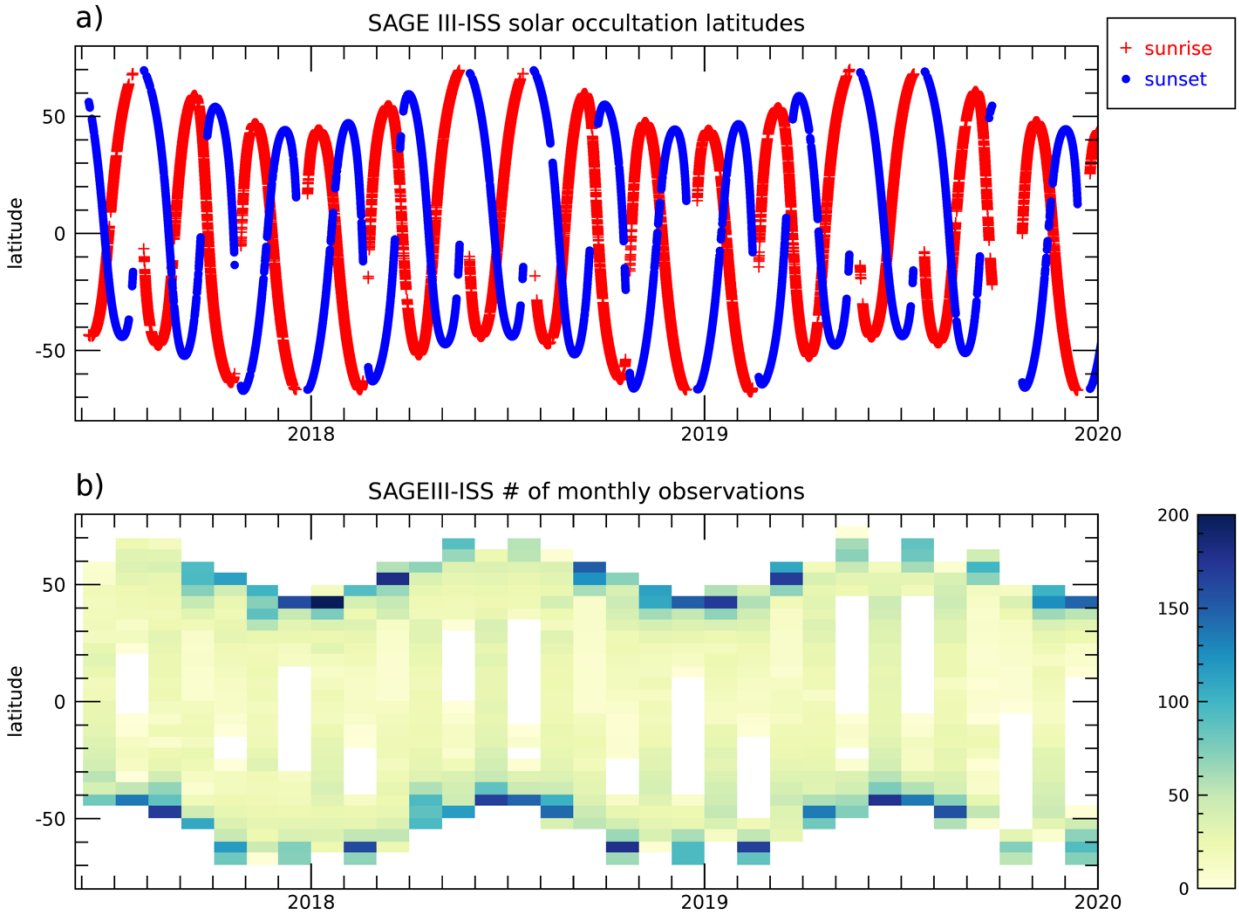

Figure 1. **a)** SAGE III/ISS solar occultation latitudes as a function of latitude and time, separated by event type (sunrise and sunset). **b)** The number of SAGE III/ISS solar occultation measurements as a function of latitude and time, in monthly 5° latitude bins. Data shown are from the mission start (June 2017) through December 2019.

3 Correlative data and methods

3.1 Aura MLS

The Aura Microwave Limb Sounder (MLS) instrument began taking data in August 2004 from aboard the NASA Earth Observing System Aura satellite (Waters et al., 2006). MLS measures thermally emitted microwave radiation from Earth's limb, and retrieves water vapor using the 190 GHz channel (Lambert et al., 2007; Read et al., 2007). MLS achieves nearly global coverage (82°S - 82°N), sampling ~3500 profiles per day with a vertical resolution of 2.5 – 3.5 km for stratospheric water vapor (100 hPa – 1 hPa). Here, we use version 4.2 data, which are provided at 12 levels per decade (~ 1.25 km) for pressures greater than 1 hPa. Over this range, the estimated accuracy (precision) for water vapor ranges from 4 to 19% (4 to 15%, Livesey et al., 2020). MLS data are screened according to the recommendations in the Aura MLS version 4.2 data quality document (Livesey et al., 2020).

3.2 ACE-FTS

The Atmospheric Chemistry Experiment Fourier Transform Spectrometer (ACE-FTS) is a solar occultation limb sounder launched in 2003 aboard the SCISAT satellite. ACE-FTS measures mid-infrared radiances (750 – 4400 cm^{-1}) with a vertical field of view of ~3 to 4 km to retrieve numerous trace gases on a 1 km altitude grid. Measuring since February 2004, ACE-FTS observes up to 30 solar occultation events per day, with sampling focused on high latitudes due to its high inclination orbit (74°). In this paper, we use both ACE-FTS v3.6 data, which is a minor update to the validated v3.5 data (Boone, 2013; Sheese et al., 2017), and the recently released v4.1 data (Boone et al., 2020). The newest version of ACE-FTS is included here to assess any potential differences between it and the well validated earlier version of the data. Validation efforts for ACE-FTS v3.5 data have demonstrated that the water vapor product has good stability and mean bias within 10% (17-70 km) in comparison to the Michelson Interferometer for Passive Atmospheric Sounding (MIPAS) and Aura MLS measurements (Sheese et al., 2017). The assessment of ACE-FTS data in WAVAS-II also corroborates these results (Khosrawi et al., 2018; Lossow et al., 2019).

3.3 Frost point hygrometer measurements

The balloon-borne frost point water vapor measurements used here consist of NOAA Frost Point Hygrometer (FPH, Hurst et al., 2011) and Cryogenic Frostpoint Hygrometer (CFH, Vömel et al., 2007) soundings at 5 sites (see Table 1) during both routine monthly soundings and specially chosen times to correspond to ISS overpasses. The CFH and NOAA FPH use the same basic principle to measure frost point temperatures at high vertical resolution (~5 m), but there are subtle differences in the way they operate. Each uses a different optical system and control parameters to regulate a thin layer of ice on a temperature-controlled mirror, and there are also differences in the way unwanted stray light (i.e., sunlight) is filtered. Several dual flights of the two hygrometers since 2005 have demonstrated their agreement is well within the stated measurement uncertainties (< 10%), especially in the stratosphere (Hall et al., 2016; Vömel et al., 2007).

Table 1. Frost point hygrometer soundings used in this study (17 June 2017 to 31 December 2019)

Station	Instrument	Latitude	Longitude	# Soundings	# SAGE coincidences
Lindenberg (GER)	CFH	52.2	14.1	64	14
Boulder (USA)	FPH	40	-105.2	38	23
Hilo, HI (USA)	FPH	19.7	-155.1	28	9
San Jose (CRI)	CFH	10	-84.1	29	9
Lauder (NZL)	FPH	-45	169.7	28	13
TOTAL				187	68

3.4 Coincident profiles

For identifying coincident measurements from correlative data sources, it is necessary to define coincidence criteria since measurements are generally not made at the exact time and geographical location. Here, we use criteria very similar to that used by Wang et al. (2020) to identify matched pairs of ozone profiles from SAGE III/ISS and correlative satellite data sets.

For matching other satellite data sets with SAGE III/ISS, we consider profiles to be matched with SAGE III/ISS if they fall within ± 1 day, ± 2° latitude, and ± 1113 km in longitude (i.e., equivalent to ± 10° longitude at the equator). For the case of multiple correlative profiles meeting this match criteria, the profile with the closest spatial distance is chosen.

For matching with frost point hygrometers, we use a relaxed coincidence criteria of ± 2 days, ± 4° latitude, and ± 2226 km zonally (i.e., equivalent to ± 20° longitude at the equator). These relaxed criteria lead to 36% of frost point (FP) profiles obtained at the 5 sites between the start of SAGE III/ISS data and the end of 2019 being matched with SAGE, as opposed to 16% when the more restrictive criteria are used. Of the matched FP-SAGE measurements, the median separation is 350 km and the root-mean-square time difference is 26 hours. Also, it is worth noting that 32 of the 187 FP profiles collected between the beginning of SAGE III/ISS data collection and the end of 2019 were purposefully timed with SAGE III/ISS solar occultation overpasses to obtain matched data, so in general these measurements are quite well matched with SAGE occultations.

4 SAGE III/ISS data quality screening criteria

4.1 Known anomalies and outliers in version 5.1

As of the end of 2019, SAGE III/ISS has collected 21,879 solar occultation profiles of water vapor, all of which are shown in Figure 2. An analysis of these reveals a number of anomalous profiles that can be broken into two categories: failed retrievals and “keel-over” profiles. Both of these anomalies have a similar cause. The amount of extinction from water vapor in the spectral region surrounding 945 nm is very small in the upper stratosphere and mesosphere and the SAGE III/ISS water vapor retrieval uses a non-linear onion peeling technique, meaning it starts at the top of the profile and iteratively works its way down while using the previous solutions for the next iteration. With a weak signal and a non-linear solution, instabilities can arise that result in mixing ratios that tend to oscillate back and forth between very large positive and very large negative through the onion peeling process. This oscillatory behavior, a byproduct of error propagation (Clarmann et al., 1991), is a common outcome of any onion peeling retrieval in a weak signal regime and results in a noisy solution at the top of the profile that relaxes with decreasing altitude. Occasionally the solution arrives at a negative value that is so large it cannot properly recover, resulting in the anomalous profiles shown in red in Figure 2a. Similarly, the solution sometimes arrives at a very large positive value that it slowly relaxes from as the retrieval moves to lower altitudes, resulting in the “keel-over” profiles, so named because the mixing ratio appears to keel over towards very large values in the upper part of the profile.

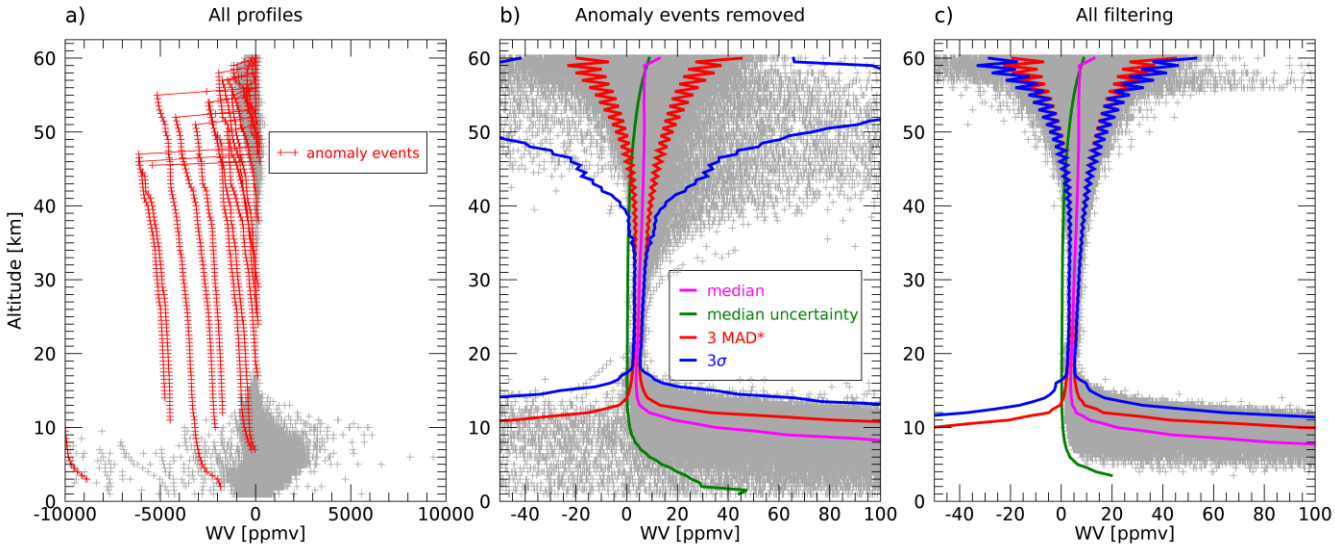

Figure 2. a) All retrieved water vapor values collected by SAGE III/ISS through the end of 2019 (gray +). Anomalous water vapor profiles are shown in red (see Table 2), and have been removed in the middle and right panels. **b)** SAGE III/ISS WV values on an enlarged scale, along with the median values (magenta), median uncertainties (green), and two diagnostics of the dispersion of the data: the median ± 3-standard deviation lines (blue) and corresponding 3 times the scaled median absolute deviations (MAD*=1.48*MAD, red). **c)** SAGE III/ISS WV values after removal of anomalous profiles (Section 4.1), keel-over profiles (Section 4.2), and aerosol/cloud contaminated data (Section 4.3).

In version 5.1, the data are screened for failed retrievals or obviously unphysical results by the SAGE team prior to their release as part of a Quality Assurance (QA) step that was also done during the SAGE III/M3M mission. The large, unphysical, negative anomalies are intentionally removed during the QA step, but this is still a manual process and, as evident by Figure 2a, sometimes an error is made and failed retrievals slip through for release to the public. A list of these missed anomalies identified for manual removal is shown in Table 2. Also included in this list of bad events is one profile affected by solar eclipse conditions (i.e., with bit flag 6 set, see NASA, 2018).

Table 2. Anomalous water vapor events in SAGE III/ISS version 5.1 (17 June 2017 to 31 December 2019)

Event number	Date	Time	Latitude	Longitude	Reason
1128120	2018-05-11	12:51:54	-39.97	60.35	anomaly
1495410	2019-01-02	16:59:41	43.92	-139.92	anomaly
1587720	2019-03-03	3:01:49	-54.70	-122.50	anomaly
1587920	2019-03-03	6:07:17	-54.45	-169.04	anomaly

1589520	2019-03-04	6:50:56	-52.29	178.72	anomaly
1592220	2019-03-06	0:34:43	-48.09	-89.27	anomaly
1596720	2019-03-08	22:08:09	-39.07	-55.50	anomaly
1630910	2019-03-30	22:05:22	-43.44	123.49	anomaly
1632310	2019-03-31	19:44:11	-45.70	159.39	anomaly
1683520	2019-05-03	18:50:00	-46.95	-30.86	anomaly
1739820	2019-06-09	0:20:16	33.84	-78.85	anomaly
1756710	2019-06-19	22:29:33	-1.39	113.57	anomaly
1762620	2019-06-23	17:13:27	-32.26	-3.68	anomaly
1766110	2019-06-25	22:25:57	28.04	100.89	anomaly
719620	2017-08-21	20:23:56	-6.69	-36.65	eclipse

While the large, unphysical, negative anomalies were intentionally, though incompletely, removed during the QA process, the keel-over profiles were intentionally left in the data set. This was so these events could be evaluated by the users to determine if the data below the keel were usable. Keel-over events are easily identifiable by large statistical outliers in the upper stratosphere in Figure 2b and are responsible for the divergence above ~35 km between the standard deviation (blue line in Figure 2b) and the scaled median absolute deviation (red line in Figure 2b), which is an outlier resistant measure of the dispersion in data (Leys et al., 2013). For a normal distribution, the MAD is directly related to the standard deviation by a scale factor of 1.48, so in Figure 2 we plot the scaled MAD (i.e., MAD* = 1.48*MAD) for comparison with the standard deviation. For a normal distribution with outliers, the standard deviations are larger than the scaled MADs and is a poor measure of the dispersion in the data. The fact that the two diagnostics are in good agreement in the lower-to-middle stratosphere suggests that the data below the keel of keel-over events may still be of good quality. A method of diagnosing these events and filtering out the keel-over portion is discussed in Section 4.2.

Apart from the known anomalies discussed above, there are other statistical outliers in the upper troposphere (below ~15 km), again evidenced by the dispersion between the standard deviations and the scaled MADs. While some of this is attributable to increasing geophysical variability with decreasing altitude in this region, negative values of water vapor are not expected in the troposphere. Instead, these outliers are likely to occur due to contamination of the transmission profiles by clouds. Solar occultation retrievals assume spherical homogeneity of the atmosphere (i.e., a concentration of a species is constant for a given altitude). While this assumption generally breaks down further in the troposphere, it is particularly incorrect in the presence of clouds. This causes the data obtained when viewing a cloud to corrupt the data obtained below it during the inversion process, producing statistical outliers that are both positive and negative. As such, simply removing negative values would be insufficient which is why it has always been recommended to ignore data below the top of a cloud obtained from occultation instruments. A technique for filtering this data is discussed in Section 4.3.

While negative values are not expected in the troposphere, where water vapor values are typically large, they can be present as a result of noise in the weak signal regime (i.e., in the upper stratosphere). This is clearly shown by the increasing reported uncertainties (green line in Fig. 2b) and increasing spread of the scaled MADs (red line in Fig. 2b) in the upper stratosphere

that encompasses negative values. The oscillatory pattern in the MADs is a result of the retrieval being performed on a 1 km grid and interpolated to the 0.5 km grid, thus making the outer envelope of the MADs indicative of the spread in the retrieved data while the inner envelope is a result of the interpolation that acts like a form of smoothing in the presence of oscillatory noise patterns from onion peeling. It is generally recommended to not attempt to filter out negative values (or values with large uncertainties) in the presence of noise (such as in the upper stratosphere), as doing so has the potential to bias spatially averaged data (e.g., zonal means) high.

After applying the filtering described in the next two sections, the SAGE III/ISS data set is much more well behaved, as illustrated in Figure 2c. For example, both the 3σ and MAD* estimates are in agreement in the upper stratosphere, indicating successful removal of the outlier values in this region. Also, outliers in the upper troposphere (both negative values and large positive outliers) are removed.

4.2 Filtering keel-over profiles

As mentioned in Section 4.1, keel-over profiles in the SAGE III/ISS WV data manifest as a systematic increase in WV value upwards along the profile, as illustrated in the example shown in Figure 3. In these profiles, there is a strong vertical gradient in water vapor that leads to a large positive peak in the profiles, often followed by an oscillation and large negative peak above that (see example in Figure 3a).

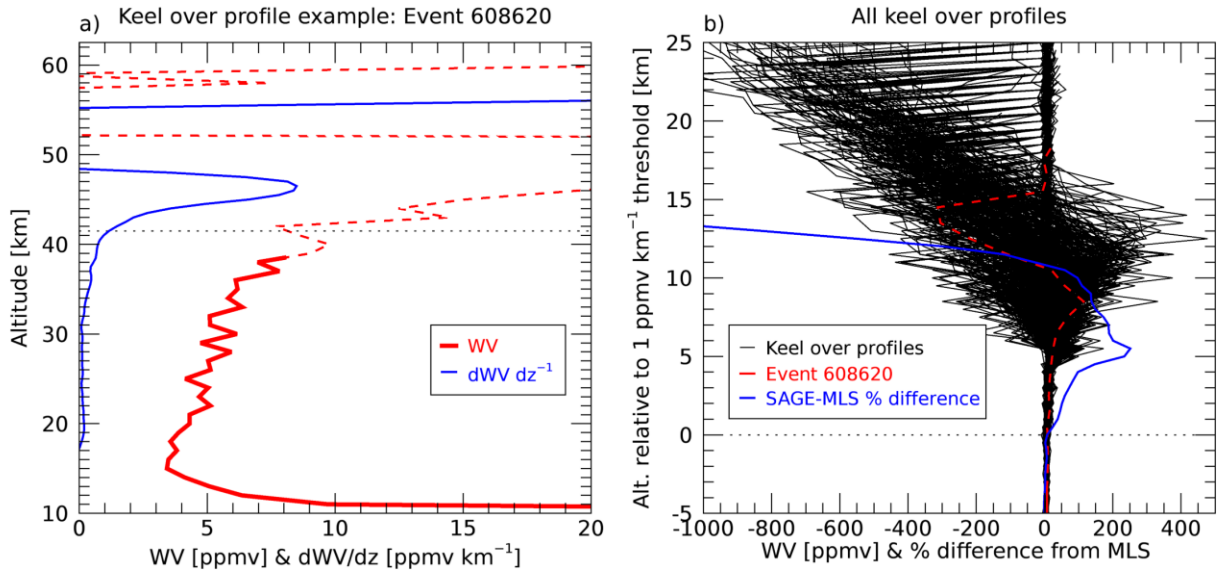

Figure 3. a) An example keel-over profile from event #608620 taken on 2017-06-11 at 11:10:14 UTC (46.3° N, 128.9° E). The thick red line is retained, and the dashed line is removed using the keel-over filtering described in Sect. 4.2. **b)** A plot of all 573 keel-over profiles identified in the SAGE III/ISS data through 2019 (black lines). Also highlighted in red is the event from **a)**, as well as the mean percent differences from MLS for the keel-over profiles (blue). In both plots, the horizontal dotted line indicates the level at which the vertical derivative of water vapor reaches 1 ppmv km^{-1}.

The general strategy for identifying keel-over profiles is to find the presence of a large positive vertical gradient in water vapor (dWV/dz), and then remove the part of the profile above the point where this occurs. Because of noise in the profiles, particularly in the mid and upper stratosphere where keel-overs occur, we smooth the profiles before computing the vertical derivatives. Through experimenting with different averaging and vertical derivative thresholds, we found that a 5 km boxcar average and derivative of 1 ppmv km^{-1} adequately identifies keel-over profiles without creating too many false positives. To be conservative in the filtering, we remove the portion of the profile above the level 2.5 km below the point at which the smoothed derivative is 1 ppmv km^{-1} (see dashed red lines in Fig. 3 showing the removed portion of the profile).

In this filtering, we are assuming that the bottom part of the keel-over profile is of reasonable quality, which is a reasonable assumption since the retrieval iterates from the top of atmosphere downwards and the retrieval instability occurs in the tops of these profiles. However, to test this we compared the 573 keel-over profiles to their closest matched MLS profiles to verify that the SAGE III/ISS data problems occur above the 1 ppmv km^{-1} point. Indeed, the mean percent differences from MLS (blue line, Figure 3b) only appears to show extreme deviations near and above the 1 ppmv km^{-1} level, not in the lower part of the profile.

4.3 Filtering of data affected by clouds

In general, SAGE III/ISS water vapor data become unusable in the presence of clouds. This is both within the cloud, where the LOS optical depth becomes so large that the water vapor signal is comparatively too weak to retrieve, and below the cloud, where the assumption of atmospheric spherical homogeneity corrupts data during the inversion process. For previous SAGE data, these points were identified through the use of the visible (525 nm) and/or near-infrared (1020 nm) aerosol extinction values, and techniques could be simpler (e.g., Kent et al., 1993) or more complicated (e.g., Thomason & Vernier, 2013). Recommendations for ozone have traditionally relied on the extinction "color ratio" (β_{1022} / β_{520}); values of color ratio ~0.2 – 0.4 are typical for stratospheric aerosols, and values greater than ~ 0.5 are indicative of large (> 1 μm) cloud particles. For this study, we do not attempt to create a robust analysis to differentiate between aerosol and cloud; instead we simply wish to implement a set of filtering criteria that aggressively attempts to filter out cloud-like influences that would detrimentally impact retrieved water vapor.

For SAGE III/ISS data, we consider both color ratio and extinction for filtering bad WV data in the troposphere, since the combination more clearly isolates the cloud-affected portion of the data. This separation is illustrated in Figure 4, which shows the distributions of 1022 nm extinction and color ratio as a function of altitude, and their joint distribution for data below 20 km. Filtering solely based on extinction is not straightforward, because at a given altitude the distribution is unimodal with a long tail (see Figure 4a); this makes identification of a threshold extinction value difficult. However, for color ratio (Figure 4b), the distribution is bi-modal, with one mode around 0.3 and another mode near 1.0. Similarly, for the joint distribution of 1022 nm extinction and color ratio, there is a separate mode containing large values of both extinction and color ratio that is likely due to clouds (upper right, Figure 4c).

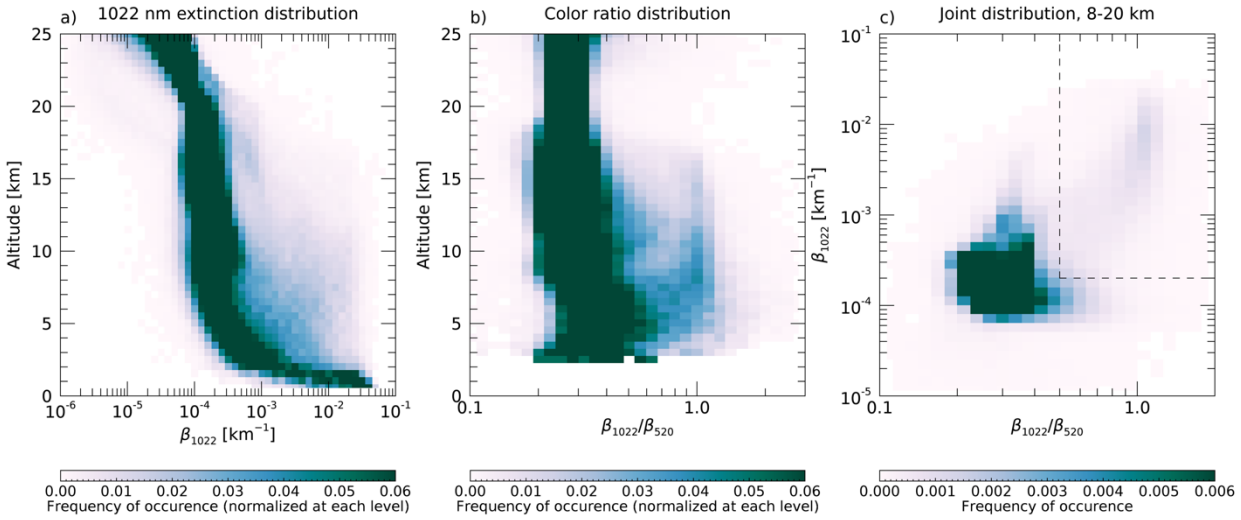

Figure 4. a) The frequency of occurrence histogram of extinction and **b)** color ratio in SAGE III/ISS data, normalized at each vertical level. **c)** The joint distribution of 1020 nm extinction and color ratio. The dashed line illustrates the threshold chosen for screening SAGE III/ISS WV data based on extinction and color ratio, as described in the text.

Next, we test how removing the presumed cloud-affected data affects the large number of negative SAGE III/ISS WV values in the troposphere and the comparison with MLS in this region. To filter out the affected data, for each profile we discard WV values below the point 1 km above the highest level at which both the color ratio is greater than 0.5 and the 1022 nm extinction is greater than 2 x 10^{-4} km^{-1}. These thresholds are illustrated as dashed lines in the joint distribution in Figure 4c. Discarding data 1 km above the level of this exceedance is done because of the smoothing applied to the measured transmission profile during the water vapor retrieval. In addition to the extinction/color ratio filtering, we also discard WV values below the point 1 km above the highest level at which an invalid/fill value occurs in extinction from either the 520 or 1022 nm channel, for levels at and below 19 km. These fill values typically occur when the line-of-sight optical depth becomes large enough to cause the retrieval to terminate in a channel, and are typically indicative of clouds along the line of sight. It is perhaps obvious but worth noting that this additional filtering is necessary because it is not possible to apply the aforementioned color ratio and extinction filtering when one or both of the channels contains a fill value.

Overall, the cloud filtering removes 35% of the SAGE III/ISS WV data below 19 km, including almost all of the negative WV values in this region (e.g., Figure 1). Figure 5 illustrates the impact of this filtering on comparison of SAGE WV data with matched MLS profiles. As can be seen in this figure, the largest differences occur at higher values of color ratio, and these outliers are successfully removed by the filtering (red points in Fig. 5). It is worth noting that these filtering criteria are inherently conservative in that they are likely removing some valid SAGE III/ISS WV values, as evidenced by the large number of data points that are removed yet in reasonable agreement with MLS. While the overall agreement with MLS is improved by this aggressive filtering, we do not further evaluate the accuracy of the tropospheric SAGE III/ISS WV data due to large uncertainties in the MLS data and high intrinsic variability of WV in this

region. Furthermore, SAGE III/ISS WV profiles often "turn over" and decrease with decreasing altitude for a few kilometers below their maximum value at the bottom of the retrieved profile, without any other obvious indications of a problematic retrieval. We do not attempt to remove these artifacts, and caution users in general regarding using SAGE III/ISS WV data in the troposphere. Finally, while the filtering described in this section removes almost all negative WV values from the SAGE III/ISS data, a few values (~ 10 for the dataset considered here) remain below 19 km. We therefore recommend that users also manually remove data below the point 1 km above the occurrence of any negative WV value occurring below 19 km.

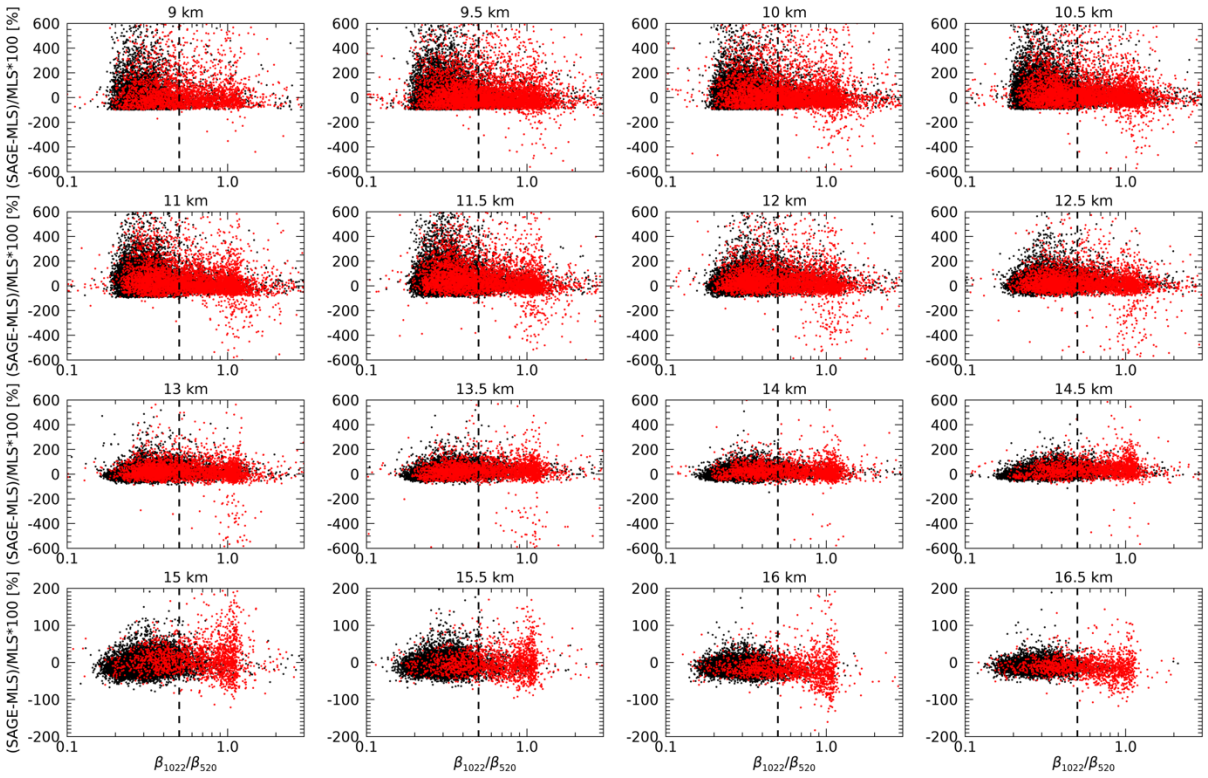

Figure 5. Percent difference of SAGE III/ISS from MLS at select levels in the upper troposphere as a function of color ratio. Black dots show all data, and red dots show data removed by the extinction and color ratio filtering described in the text.

5 Comparisons between SAGE III/ISS and correlative data sets

5.1 Satellite data: basic comparisons

In this section, we present comparisons of SAGE III/ISS WV data with correlative satellite data from Aura MLS and ACE-FTS. These comparisons are done after the quality control screening from Sect. 4 has been applied to the SAGE III/ISS data.

Of the 21,879 solar occultation profiles collected by SAGE III/ISS by the end of 2019, over 20,000 of these profiles have a matched MLS profile meeting the coincidence criteria described in Sect. 3.3. As illustrated in Fig. 6., SAGE III/ISS water vapor values are consistently

drier than MLS in the lower to mid stratosphere, where the SAGE III/ISS uncertainty is smallest (see black dash-dot line in Fig. 6b). In the median, SAGE III/ISS water vapor values are 0.5 ppmv (10 %) drier than MLS over the 15 – 35 km altitude range. Above ~35 km, the SAGE III/ISS uncertainties increase with increasing altitude (black dash-dot line in Fig. 6b), with the same being true for MLS above ~48 km (purple dash-dot line in Fig. 6b). As a result, the median difference between SAGE III/ISS and MLS changes with altitude above ~45 km.

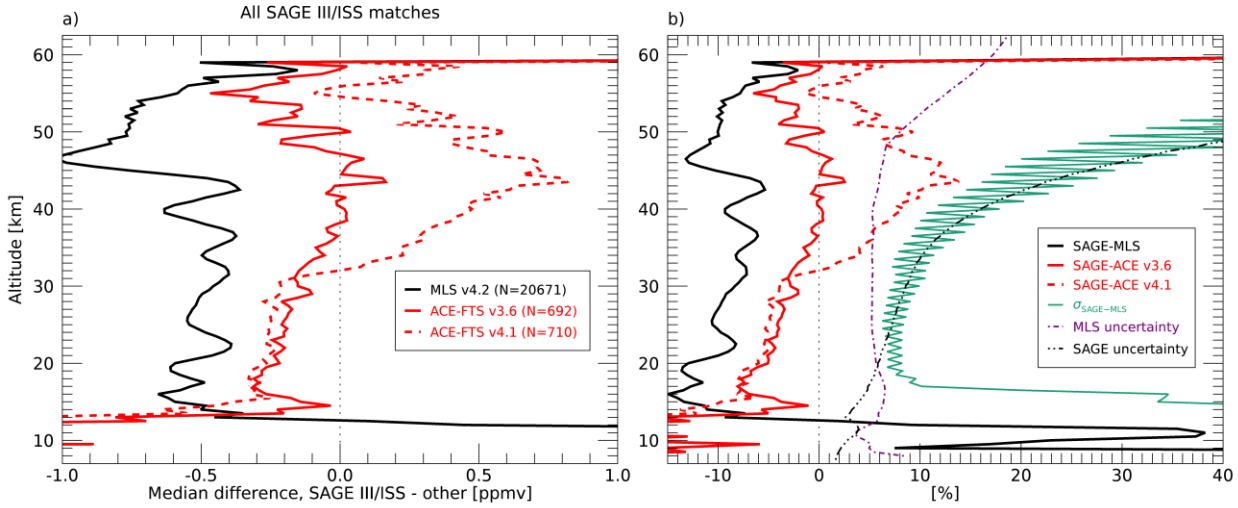

Figure 6. a) The median absolute difference between matched pairs of SAGE III/ISS and Aura MLS (black) or ACE-FTS (red). **b)** The median percent difference between SAGE III/ISS and these other satellites (defined as [SAGE-other]/other*100, black and red lines), the standard deviation of these differences (green line), and the median uncertainties for SAGE III/ISS (black) and Aura MLS (purple).

In comparison with ACE-FTS, SAGE III/ISS data are consistently drier below 30 km. In the 20 – 30 km range, SAGE III/ISS is 0.1 - 0.3 ppmv drier than both versions of ACE-FTS. Below ~15 km, SAGE III/ISS becomes significantly drier than ACE-FTS, but wetter than MLS. However, there are many caveats in these comparisons, including increased geophysical variability in this region, larger vertical gradients in water vapor which can exacerbate differences due to differing spatial resolution among the instruments, and the known “turn over” in SAGE III/ISS WV values discussed in Sect 4.3. Above 30 km, the behavior of the two versions of ACE-FTS is quite different. Version 4.1 transitions to having a positive bias with increasing altitude, whereas v3.6 is more consistent with altitude. The behavior of v4.1 has not been fully explored at this time, so for the remainder of the paper we use the more extensively validated v3.6.

Interestingly, the standard deviation of the percent difference between SAGE and MLS, which is a combination of the precision of each instrument and the geophysical variability between their coincident locations, tracks quite closely with the SAGE uncertainty above ~25 km. This suggests that random atmospheric variability between the SAGE/MLS measurement pairs is not a major contributor to the observed differences at these levels, and that the reported

SAGE III/ISS uncertainties are reasonable. In contrast, below 18 km the standard deviation of the SAGE/MLS difference grows rapidly with decreasing altitude, due to increased atmospheric variability in the upper troposphere lower stratosphere (UTLS) region.

Another important consideration in how SAGE III/ISS compares to other data sets is whether or not there are noticeable geographic variations in the comparison. Figure 7 shows the comparison between SAGE III/ISS and MLS as a function of both height and latitude, along with the thermal tropopause computed from the Modern-Era Retrospective analysis for Research and Applications, Version 2 (MERRA-2) reanalysis (Gelaro et al., 2017). This figure indicates that the SAGE III/ISS dry bias (relative to MLS) is consistent with latitude throughout most of the overworld stratosphere above ~ 15 km. There are several geographical regions with less consistency that are worth pointing out. First, in the high latitude lower stratosphere, there are regions where SAGE III/ISS is significantly drier than MLS. This region may be influenced by aerosol contamination from volcanoes and fires, as will be discussed in the next section. These pockets of strong dry bias are also likely related to problems with the MLS water vapor in these regions at the 147 and 121 hPa levels, as discussed in Davis et al. (2016). Similarly, the transition to positive biases in the UTLS region is consistent with the known Aura MLS dry bias in this region (Davis et al., 2016; Vomel et al., 2007). At latitudes poleward of ~45° in each hemisphere, this transition occurs above the tropopause, as can be seen in the green banding in Fig. 7 above the tropopause (dashed and solid lines) in each hemisphere. It is worth stressing that the transition to positive bias in the UTLS is also large in percent difference (Fig. 7 b), and is not merely the result of moving into a region where the water vapor values are larger (i.e., where a 1 ppmv bias would be relatively small). Finally, it is worth noting that above 45 km the loss of precision in MLS but especially SAGE III/ISS (see, e.g., Fig. 6b) leads to increased noise in the comparison shown in Fig. 7.

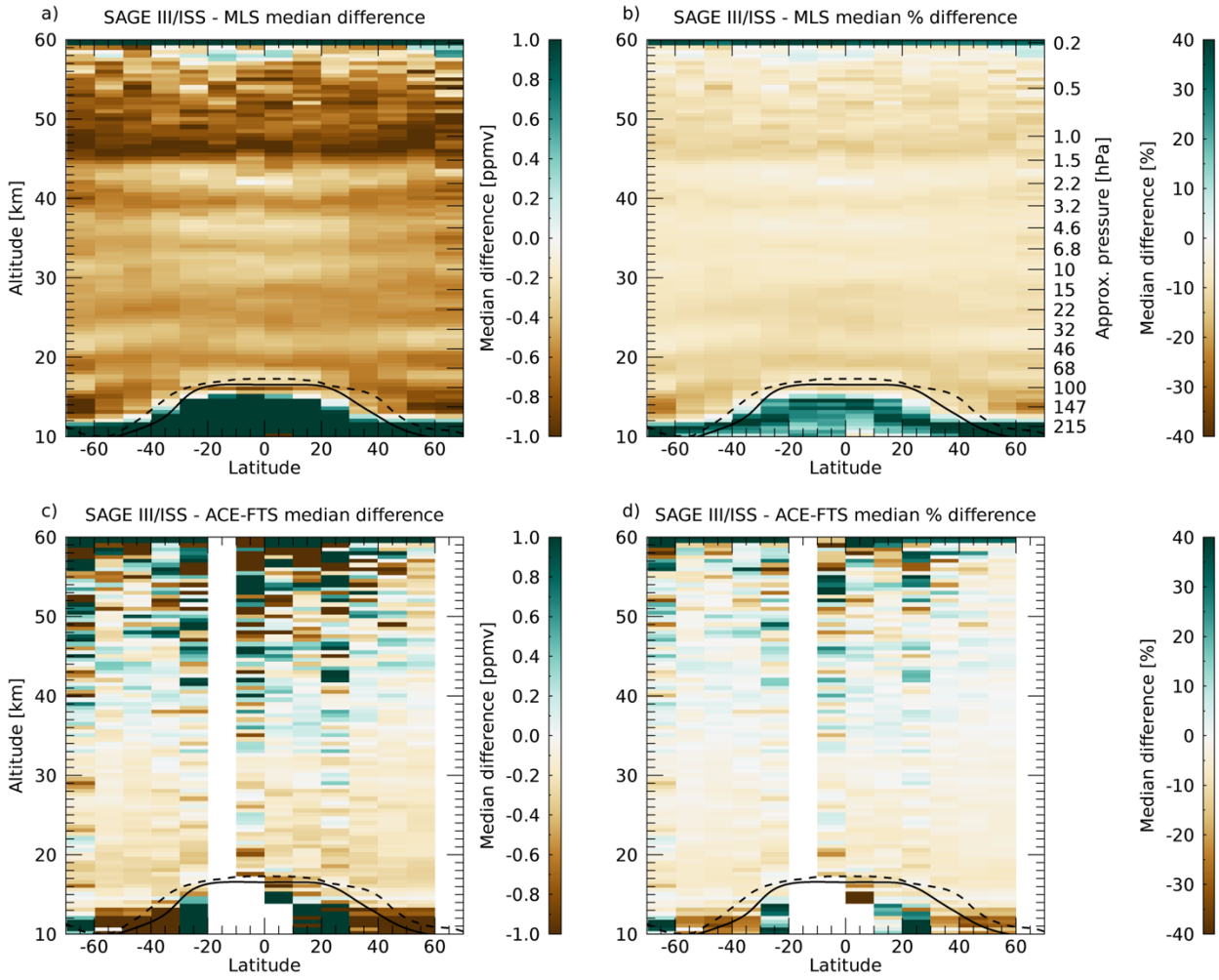

462

463 **Figure 7. a)** The median difference of SAGE III/ISS minus Aura MLS and **b)** median percent
464 difference as a function of altitude and latitude. The corresponding plots for ACE-FTS v3.6 are
465 shown in the bottom row (panels c and d, respectively). The mean (solid) and maximum (dashed)
466 thermal tropopause height over the SAGE III/ISS time period (2017-06 through 2019-12) from
467 the MERRA-2 reanalysis is shown in all panels.

468

469 The comparison with ACE-FTS v3.6 in Figure 7 reinforces the behavior apparent in Fig.
470 6. Through most of the stratosphere SAGE III/ISS is dry-biased relative to ACE-FTS, with a
471 decrease in this bias at higher altitudes. Interestingly, there is a suggestion of a latitude-
472 dependence of this bias, with SAGE III/ISS showing relatively wetter values at low latitudes and
473 drier values at high latitudes, in comparison to ACE-FTS. However, it should be stressed that
474 given the predominant high latitude sampling from ACE-FTS, the number of matched profiles in
475 the tropics (N=74, 30°S – 30°N) for these comparisons is significantly lower than at high
476 latitudes (N=658 for |lat| > 30°).

5.2 Satellite comparisons: sensitivity to aerosol

In the lower stratosphere, near or above the hygropause, water vapor is not the primary contributor to the overall extinction in the spectral region surrounding 945 nm. Instead, it can vary considerably with aerosol loading levels and ranges from ~10% at "background" conditions down to ~1% after a major volcanic eruption (Thomason et al., 2004). Studies of previous SAGE instruments looked at the sensitivity of the water vapor product and noticed biases with other measurement systems, recommending filtering criteria based on overall aerosol loading levels. As an example, for SAGE II water vapor data, Taha et al. (2004) recommended removing data in profiles below the highest altitude at which β_{1022} (1022 nm extinction) was greater than 2×10^{-4} km^{-1}. Herein we investigate the sensitivity of SAGE III/ISS water vapor to aerosol loading in the lower stratosphere using coincident Aura MLS data surrounding five stratospheric aerosol injections since the start of the SAGE III/ISS mission.

Over its first three years, SAGE III/ISS has observed several small volcanic eruptions (i.e., Ambae in 2018 and Ulawun and Raikoke in 2019) and the two largest pyrocumulonimbus (PyroCb) clouds ever recorded (i.e., Canadian wildfires in 2017 (Yu et al., 2019) and Australian bushfires in 2019/2020 (Kablick et al., 2020)). Unlike during SAGE III/M3M, which observed a relatively clean stratosphere that did not appear to impact water vapor (Thomason et al., 2010), these events present an opportunity to assess the impact that moderately elevated aerosol loading has on the retrieved water vapor. Figure 8 looks at the difference between SAGE III/ISS and MLS water vapor between 14 and 24 km as a function of integrated aerosol optical depth near 1 µm in the months after three volcanic eruptions (Ambae, Ulawun, and Raikoke) and the two major PyroCbs. These data show a systematic negative bias in the SAGE III/ISS data that worsens with increasing aerosol loading. At these altitudes and elevated loading levels, the contribution of aerosol to the overall extinction near the peak of water vapor absorption in the SAGE channel can be 50 times larger than that of water vapor itself.

Furthermore, it appears that the systematic change in the bias is more pronounced with smaller particles (e.g., volcanic events) than with larger particles (e.g., the fires). This may be because the SAGE retrieval attempts to solve for water vapor, ozone, and aerosol all at once. Sulfate aerosol (from volcanic eruptions) exhibits a larger dependency of extinction with wavelength than smoke aerosol. This enhanced slope can potentially alias into the other terms of the retrieval such as the wings of the ozone cross-sections in the spectral region used by SAGE or into the overall slope of absorption from water vapor. The SAGE team is currently investigating this effect in an effort to correct it in a future version.

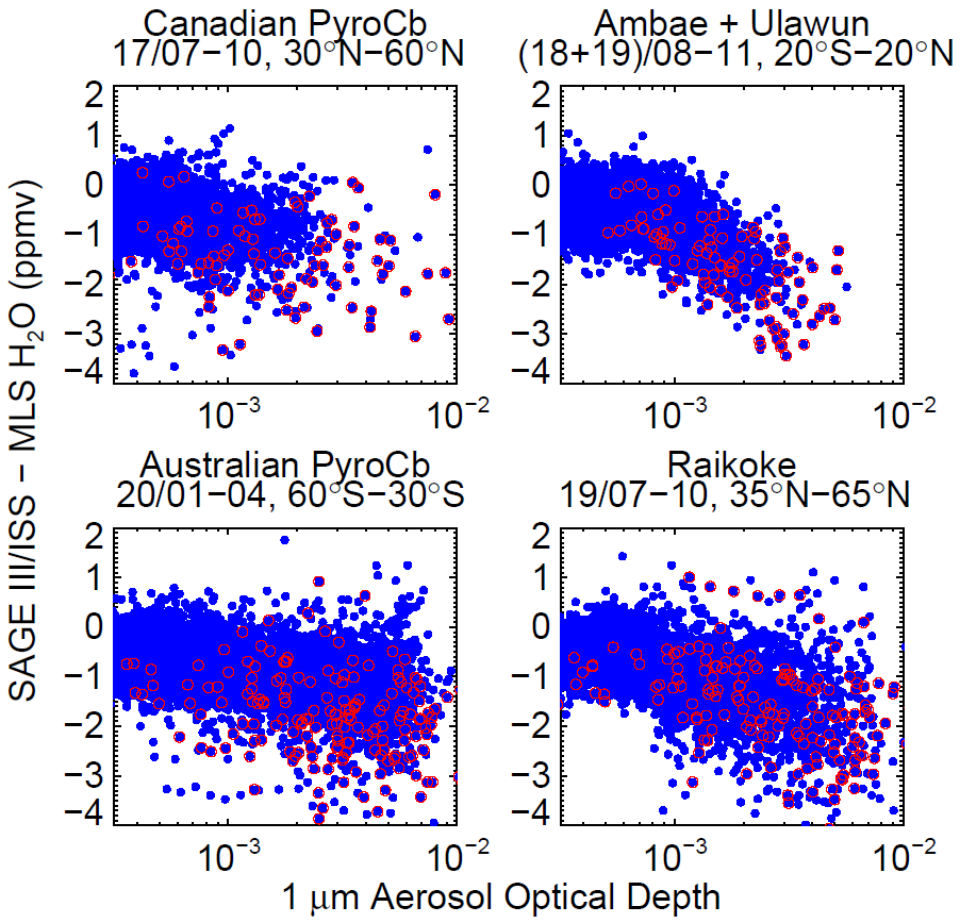

Figure 8. Difference between SAGE III/ISS and MLS WV as a function of SAGE 1 μm aerosol optical depth (AOD) for different stratospheric aerosol injection events. Events, dates, and latitude ranges are labeled for each plot. The Ambae and Ulawun eruptions were combined because of their similar behavior. Points include all data between 14 and 24 km and actively exclude data both below the hygropause and below the peak 1 μm aerosol extinction in each profile to illustrate the impact of elevated aerosol loading on trace amounts of water vapor. Red circles are placed around values where the uncertainty in SAGE water vapor data is ≥100%.

While a negative bias of SAGE III/ISS water vapor with increased aerosol loading exists, there is no distinct transition at which this occurs. The effect is gradual, making any clear method of filtering the data difficult. Additionally, filtering the data in the same way as is done for clouds (i.e., removing all data at altitudes below some criteria) should not be necessary, as the contribution of water vapor to the overall signal increases significantly below the hygropause even with elevated aerosol loading, and any negative bias in stratospheric water vapor would have a negligible impact on the retrieval of tropospheric water vapor. That having been said, we investigate the overall change in bias with aerosol loading. Figure 9 shows both a 2D histogram of all of the differences between coincident SAGE III/ISS and MLS events as a function of 1 μm aerosol extinction and a running median of these data. It appears that at low aerosol loading levels ($\leq 10^{-4}$ km^{-1}), there is a roughly 10% offset between the two instruments, consistent with the results shown in the previous section. A -5% aerosol-induced bias (15% total offset) occurs

around 2.5×10^{-4} km^{-1} and a -10% bias occurs around 5.0×10^{-4} km^{-1} (20% total offset). It is worth noting that although the reported SAGE III/ISS uncertainties cannot themselves be used as a definitive filtering criterion, the relative uncertainties also tend to increase with increased aerosol loading (not shown), with uncertainties increasing rapidly once the 1 µm aerosol extinction exceeds 10^{-3} km^{-1}. That means the uncertainties can be used for other analyses (e.g., computing weighted versus unweighted means) to help mitigate the impact of the sensitivity of SAGE III/ISS water vapor to aerosol loading levels.

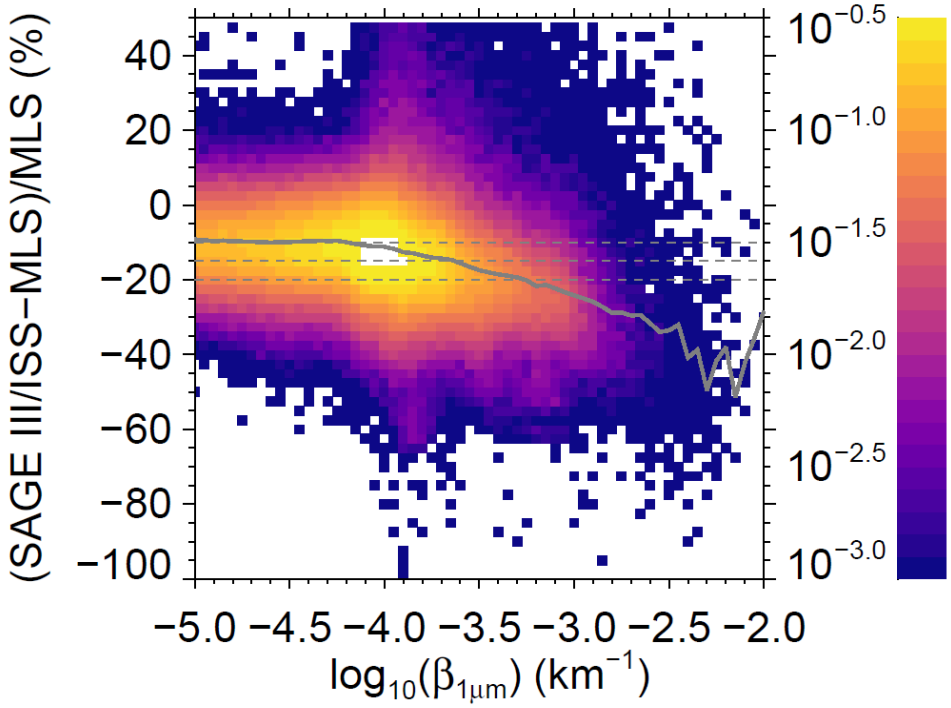

Figure 9. 2D histogram of the percent differences between SAGE III/ISS and MLS as a function of 1 µm aerosol extinction. The data is for all altitudes between 14 and 30 km and for all coincident events between June 2017 and May 2020 and the color scale shows the fractional percentage of data points in each bin. The gray line is a running median of the data showing how the overall negative bias increases with increasing aerosol loading.

5.2 Frost point hygrometer soundings

Balloon-borne frost point hygrometer data offer the opportunity to compare SAGE III/ISS water vapor data to independent measurements that have been extensively used for comparisons to other satellite data sets, including both Aura MLS and previous SAGE instruments (e.g., Davis et al., 2016; Read et al., 2007; Vomel et al., 2007). Since frost point measurements are made at much higher vertical resolution than SAGE, we apply a vertical smoothing to the frost point data. The smoothing used here consists of a triangular averaging window with 2 km full width at half maximum (FWHM). Although the vertical resolution of each satellite instrument is slightly different, they are all in the 2-3 km range in terms of vertical resolution.

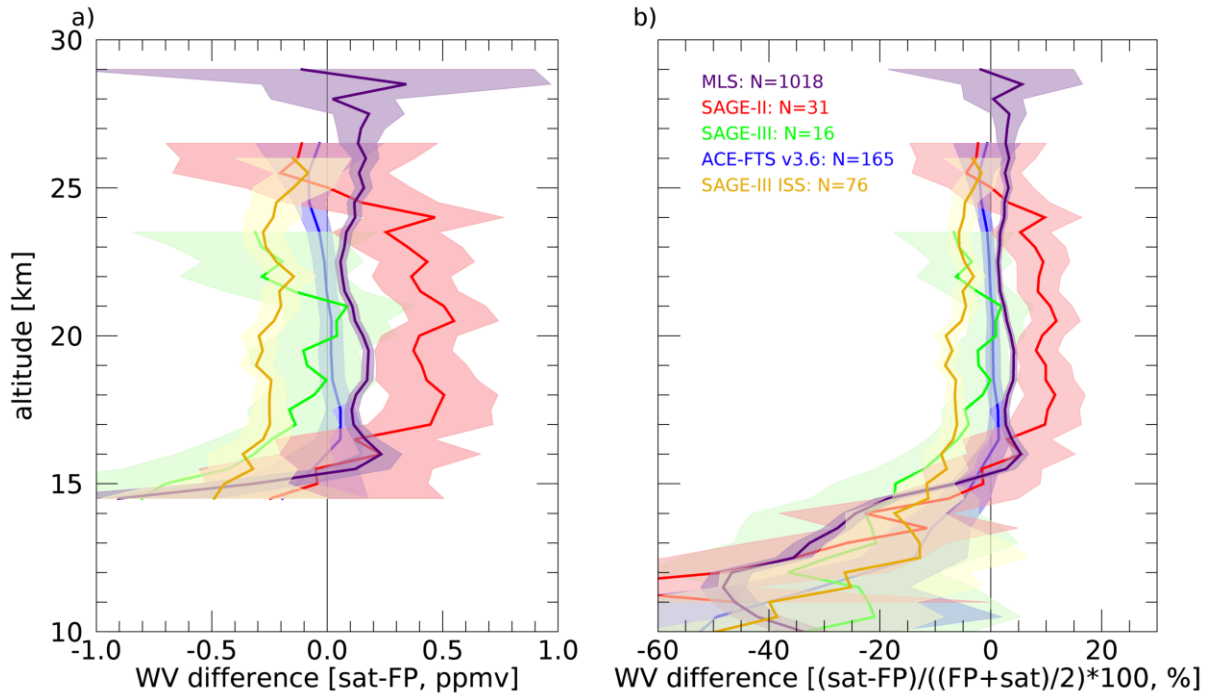

Figure 10. a) The median differences and **b)** median percent differences between various satellites and coincident frost point (FP) measurements. The shading on each instrument shows ±2 standard error estimates. In **(a)** the axis range is restricted and data are shown for levels at which the mean WV is less than 10 ppmv in order to highlight differences in the stratosphere.

In line with previous validation and intercomparison studies, Figure 10 shows that in the median the satellite data agree with the frost point measurements to within 0.5 ppmv in the stratosphere. The relative dry bias in SAGE III/ISS seen earlier in the comparisons to MLS and ACE-FTS is further borne out in this comparison. SAGE III/ISS is 0.1 – 0.3 ppmv drier than the frost points in the stratosphere, with ACE-FTS v3.6 agreeing very closely with the frost points and MLS 0.1 – 0.2 ppmv wetter, as shown by Hurst et al. (2016). In the upper troposphere, all satellite instruments are dry-biased relative to the frost points, but the usual caveats regarding comparisons in this region apply. In addition to questionable data quality and large WV gradients, the large geophysical variability coupled with relaxed matching criteria used here (see Sect 3.3) could be particularly problematic for the reliability of comparisons in this region.

6. Summary

SAGE III/ISS continues the heritage of satellite stratospheric water vapor vertical profile measurements spanning back to the 1980's, and this data set is one of only a handful of satellite limb sensors currently in operation. This paper has assessed the first publicly released beta version 5.1 in comparison to existing balloon and satellite water vapor measurement, in order to provide guidance and recommendations. Based on this analysis, we have devised a set of suggested criteria for data users in order to filter out outliers and data impacted by interference from clouds. Our recommendations are as follows:

1. Remove profiles that are obvious anomalies (events in Table 1)

2. Remove data in "keel over" profiles above the point 2.5 km below the level at which the (5 km) smoothed vertical derivative is 1 ppmv km^{-1}.
3. Remove data below the point 1 km above the level at which either criteria occur:
    a. Color ratio (β_{1022} / β_{520}) > 0.5 & β_{1022} > 2 x 10^{-4} km^{-1}
    b. Fill value for either β_{1022} or β_{520} below 19 km
    c. Negative WV value below 19 km

Additionally, users of SAGE III/ISS WV data should be aware that there may be an extinction-dependent dry bias in the data that occurs in the presence of clouds or high stratospheric aerosol loading. The source of this bias is likely algorithmic and this issue may be fixed in future versions of the data product. Also, SAGE III/ISS WV data quality in the troposphere is not fully evaluated here and should be treated with great caution. Among other potential issues, the profiles have a tendency to "turn over" and decrease with decreasing altitude for a few kilometers below their maximum water vapor value at the bottom of the retrieved profile, without any other obvious indications of a problematic retrieval.

After applying the quality control screening described herein, we find that SAGE III/ISS WV is in good agreement with independent satellite and balloon-based measurements. From 20 – 40 km, SAGE III/ISS WV v5.1 exhibit a bias of 0.0 to -0.5 ppmv (~10%) relative to ACE-FTS v3.6 and MLS 4.2 data, depending on the instrument and altitude. In comparison to frost point data from 15 – 25 km, SAGE III/ISS has a mean dry bias of 0.3 ppmv. In comparison to the other satellite instruments and the frost point balloon measurements, the SAGE III/ISS WV dry bias is very stable with altitude. It is likely that future versions of the data product with updated line parameters will improve agreement further. Despite its status as a beta version, the level of SAGE III/ISS WV agreement with independent data is similar to previous SAGE instruments, and therefore the data are suitable for extending stratospheric water vapor data records and in scientific studies of stratospheric water vapor.

Acknowledgments, Samples, and Data

The authors wish to thank the SAGE III/ISS science team and the SAGE III/ISS operations team for their work in creating the SAGE III/ISS data. The authors would also like to thank the numerous personnel involved in planning and collecting coincident balloon-borne frost point measurements timed with ISS overpass events. SAGE III/ISS is a NASA Langley managed Mission funded by the NASA Science Mission Directorate within the Earth Systematic Mission Program. Enabling partners are the NASA Human Exploration and Operations Mission Directorate, International Space Station Program and the European Space Agency. SAGE III/ISS v5.1 data are publicly available through the NASA Atmospheric Sciences Data Center (https://asdc.larc.nasa.gov/project/SAGE%20III-ISS). The Atmospheric Chemistry Experiment is a Canadian-led mission mainly supported by the Canadian Space Agency.

References

Bogumil, K., Orphal, J., Homann, T., Voigt, S., Spietz, P., Fleischmann, O. C., et al. (2003). Measurements of molecular absorption spectra with the SCIAMACHY pre-flight model: instrument characterization and reference data for atmospheric remote-sensing in the 230–2380 nm region. *Journal of Photochemistry and Photobiology A: Chemistry, 157*(2), 167-184. http://www.sciencedirect.com/science/article/pii/S1010603003000625

Boone, C. D. (2013). *Version 3 Retrievals for the Atmospheric Chemistry Experiment Fourier Transform Spectrometer (ACE-FTS)*
The Atmospheric Chemistry Experiment ACE at 10: A Solar Occultation Anthology: (Peter F. Bernath, editor, A. Deepak Publishing, Hampton, Virginia, U.S.A., 2013).

Boone, C. D., Bernath, P. F., Cok, D., Jones, S. C., & Steffen, J. (2020). Version 4 retrievals for the atmospheric chemistry experiment Fourier transform spectrometer (ACE-FTS) and imagers. *Journal of Quantitative Spectroscopy & Radiative Transfer, 247*. <Go to ISI>://WOS:000536179300001

Chu, W., McCormick, M. P., Zawodny, J., & Mauldin, L. (1997). *Stratospheric aerosol and gas experiment III* (Vol. 3117): SPIE.

Chu, W. P., & Mccormick, M. P. (1979). Inversion of Stratospheric Aerosol and Gaseous Constituents from Spacecraft Solar Extinction Data in the 0.38-1.0-Mu-M Wavelength Region. *Applied Optics, 18*(9), 1404-1413. <Go to ISI>://WOS:A1979GT17300030

Chu, W. P., & Veiga, R. (1998). *SAGE III/EOS* (Vol. 3501): SPIE.

Cisewski, M., Zawodny, J., Gasbarre, J., Eckman, R., Topiwala, N., Rodriguez-Alvarez, O., et al. (2014). *The Stratospheric Aerosol and Gas Experiment (SAGE III) on the International Space Station (ISS) Mission* (Vol. 9241): SPIE.

Clarmann, T. v., Fischer, H., & Oelhaf, H. (1991). Instabilities in retrieval of atmospheric trace gas profiles caused by the use of atmospheric level models. *Applied Optics, 30*(21), 2924-2925. http://ao.osa.org/abstract.cfm?URI=ao-30-21-2924

Damadeo, R. P., Zawodny, J. M., Thomason, L. W., & Iyer, N. (2013). SAGE version 7.0 algorithm: application to SAGE II. *Atmospheric Measurement Techniques, 6*(12), 3539-3561. <Go to ISI>://WOS:000330830900002

Davis, S. M., Rosenlof, K. H., Hassler, B., Hurst, D. F., Read, W. G., Vomel, H., et al. (2016). The Stratospheric Water and Ozone Satellite Homogenized (SWOOSH) database: a long-term database for climate studies. *Earth System Science Data, 8*(2), 461-490. <Go to ISI>://WOS:000385379700001

Dvortsov, V. L., & Solomon, S. (2001). Response of the stratospheric temperatures and ozone to past and future increases in stratospheric humidity. *Journal of Geophysical Research-Atmospheres, 106*(D7), 7505-7514. <Go to ISI>://WOS:000168189400023

Forster, P., & Shine, K. (1999). Stratospheric water vapour changes as a possible contributor to observed stratospheric cooling. *Geophysical Research Letters, 26*(21), 3309-3312.

http://apps.isiknowledge.com/InboundService.do?Func=Frame&product=WOS&action=retrieve&SrcApp=Papers&UT=000083485500026&SID=4Ac266l3LL3pmABcjJO&Init=Yes&SrcAuth=mekentosj&mode=FullRecord&customersID=mekentosj&DestFail=http%3A%2F%2Faccess.isiproducts.com%2Fcustom_images%2Fwok_failed_auth.html

Gelaro, R., McCarty, W., Suarez, M. J., Todling, R., Molod, A., Takacs, L., et al. (2017). The Modern-Era Retrospective Analysis for Research and Applications, Version 2 (MERRA-2). *Journal of Climate, 30*(14), 5419-5454. <Go to ISI>://WOS:000404018600016

Hall, E. G., Jordan, A. F., Hurst, D. F., Oltmans, S. J., Vomel, H., Kuhnreich, B., & Ebert, V. (2016). Advancements, measurement uncertainties, and recent comparisons of the NOAA frost point hygrometer. *Atmospheric Measurement Techniques*, *9*(9), 4295-4310. <Go to ISI>://WOS:000383891800002

Hurst, D. F., Oltmans, S. J., Vomel, H., Rosenlof, K. H., Davis, S. M., Ray, E. A., et al. (2011). Stratospheric water vapor trends over Boulder, Colorado: Analysis of the 30 year Boulder record. *Journal of Geophysical Research-Atmospheres, 116*. <Go to ISI>://000286757000004

Hurst, D. F., Read, W. G., Vomel, H., Selkirk, H. B., Rosenlof, K. H., Davis, S. M., et al. (2016). Recent divergences in stratospheric water vapor measurements by frost point hygrometers and the Aura Microwave Limb Sounder. *Atmospheric Measurement Techniques, 9*(9), 4447-4457. <Go to ISI>://WOS:000384009800001

Kablick, G. P., Allen, D. R., Fromm, M. D., & Nedoluha, G. E. (2020). Australian PyroCb Smoke Generates Synoptic-Scale Stratospheric Anticyclones. *Geophysical Research Letters, 47*(13). <Go to ISI>://WOS:000551465400020

Kent, G. S., Winker, D. M., Osborn, M. T., & Skeens, K. M. (1993). A Model for the Separation of Cloud and Aerosol in Sage-Ii Occultation Data. *Journal of Geophysical Research-Atmospheres, 98*(D11), 20725-20735. <Go to ISI>://WOS:A1993MJ29800033

Khosrawi, F., Lossow, S., Stiller, G. P., Rosenlof, K. H., Urban, J., Burrows, J. P., et al. (2018). The SPARC water vapour assessment II: comparison of stratospheric and lower mesospheric water vapour time series observed from satellites. *Atmospheric Measurement Techniques, 11*(7), 4435-4463. <Go to ISI>://WOS:000439842200004

Lambert, A., Read, W. G., Livesey, N. J., Santee, M. L., Manney, G. L., Froidevaux, L., et al. (2007). Validation of the Aura Microwave Limb Sounder middle atmosphere water vapor and nitrous oxide measurements. *Journal of Geophysical Research-Atmospheres, 112*(D24). <Go to ISI>://000251526400001

Leys, C., Ley, C., Klein, O., Bernard, P., & Licata, L. (2013). Detecting outliers: Do not use standard deviation around the mean, use absolute deviation around the median. *Journal of Experimental Social Psychology, 49*(4), 764-766. http://www.sciencedirect.com/science/article/pii/S0022103113000668

Livesey, N. J., Read, W. G., Wagner, P. A., Froidevaux, L., Lambert, A., Manney, G. L., et al. (2020). Version 4.2x Level 2 data quality and description document. *JPL D-33509 Rev. B*. https://mls.jpl.nasa.gov/data/v4-2_data_quality_document.pdf

Lossow, S., Khosrawi, F., Kiefer, M., Walker, K. A., Bertaux, J. L., Blanot, L., et al. (2019). The SPARC water vapour assessment II: profile-to-profile comparisons of stratospheric and lower mesospheric water vapour data sets obtained from satellites. *Atmospheric Measurement Techniques, 12*(5), 2693-2732. <Go to ISI>://WOS:000467694600001

Maycock, A. C., Joshi, M. M., Shine, K. P., & Scaife, A. A. (2013). The Circulation Response to Idealized Changes in Stratospheric Water Vapor. *Journal of Climate, 26*(2), 545-561. <Go to ISI>://WOS:000313740400012

Mccormick, M. P., Hamill, P., Pepin, T. J., Chu, W. P., Swissler, T. J., & Mcmaster, L. R. (1979). Satellite Studies of the Stratospheric Aerosol. *Bulletin of the American Meteorological Society, 60*(9), 1038-1046. <Go to ISI>://WOS:A1979HM99700003

NASA. (2018). SAGE III/ISS data products user's guide. Retrieved from https://eosweb.larc.nasa.gov/project/sageiii-iss/guide/DPUG-G3B-2-0.pdf

Read, W. G., Lambert, A., Bacmeister, J., Cofield, R. E., Christensen, L. E., Cuddy, D. T., et al. (2007). Aura Microwave Limb Sounder upper tropospheric and lower stratospheric H2O and relative humidity with respect to ice validation. *Journal of Geophysical Research-Atmospheres, 112*(D24). <Go to ISI>://000252013700010

Sheese, P. E., Walker, K. A., Boone, C. D., Bernath, P. F., Froidevaux, L., Funke, B., et al. (2017). ACE-FTS ozone, water vapour, nitrous oxide, nitric acid, and carbon monoxide profile comparisons with MIPAS and MLS. *Journal of Quantitative Spectroscopy & Radiative Transfer, 186*, 63-80. <Go to ISI>://WOS:000389011000006

Solomon, S., Rosenlof, K. H., Portmann, R. W., Daniel, J. S., Davis, S. M., Sanford, T. J., & Plattner, G.-K. (2010). Contributions of Stratospheric Water Vapor to Decadal Changes in the Rate of Global Warming. *Science, 327*(5970), 1219-1223. http://www.sciencemag.org/cgi/content/abstract/327/5970/1219

Taha, G., Thomason, L. W., & Burton, S. P. (2004). Comparison of Stratospheric Aerosol and Gas Experiment (SAGE) II version 6.2 water vapor with balloon-borne and space-based instruments. *Journal of Geophysical Research-Atmospheres, 109*(D18313). <Go to ISI>://000224409200012

Thomason, L. W., Burton, S. P., Iyer, N., Zawodny, J. M., & Anderson, J. (2004). A revised water vapor product for the Stratospheric Aerosol and Gas Experiment (SAGE) II version 6.2 data set. *Journal of Geophysical Research-Atmospheres, 109*(D6). <Go to ISI>://WOS:000220744400006

Thomason, L. W., Moore, J. R., Pitts, M. C., Zawodny, J. M., & Chiou, E. W. (2010). An evaluation of the SAGE similar to III version 4 aerosol extinction coefficient and water

vapor data products. *Atmospheric Chemistry and Physics*, *10*(5), 2159-2173. <Go to ISI>://WOS:000275505500006

Thomason, L. W., & Vernier, J. P. (2013). Improved SAGE II cloud/aerosol categorization and observations of the Asian tropopause aerosol layer: 1989-2005. *Atmospheric Chemistry and Physics, 13*(9), 4605-4616. <Go to ISI>://WOS:000318941300009

Vomel, H., Barnes, J. E., Forno, R. N., Fujiwara, M., Hasebe, F., Iwasaki, S., et al. (2007). Validation of Aura Microwave Limb Sounder water vapor by balloon-borne Cryogenic Frost point Hygrometer measurements. *Journal of Geophysical Research-Atmospheres, 112*(D24). <Go to ISI>://WOS:000252013800002

Vömel, H., David, D. E., & Smith, K. (2007). Accuracy of tropospheric and stratospheric water vapor measurements by the cryogenic frost point hygrometer: Instrumental details and observations. *Journal of Geophysical Research-Atmospheres, 112*(D8). <Go to ISI>://000245951800003

Wang, H. J. R., Damadeo, R., Flittner, D., Kramarova, N., Taha, G., Davis, S., et al. (2020). Validation of SAGE III/ISS Solar Occultation Ozone Products With Correlative Satellite and Ground-Based Measurements. *Journal of Geophysical Research: Atmospheres, 125*(11), e2020JD032430. https://agupubs.onlinelibrary.wiley.com/doi/abs/10.1029/2020JD032430

Waters, J. W., Froidevaux, L., Harwood, R. S., Jarnot, R. F., Pickett, H. M., Read, W. G., et al. (2006). The Earth Observing System Microwave Limb Sounder (EOS MLS) on the Aura satellite. *Ieee Transactions on Geoscience and Remote Sensing, 44*(5), 1075-1092. <Go to ISI>://000237167100003

Yu, P. F., Toon, O. B., Bardeen, C. G., Zhu, Y. Q., Rosenlof, K. H., Portmann, R. W., et al. (2019). Black carbon lofts wildfire smoke high into the stratosphere to form a persistent plume. *Science, 365*(6453), 587-590. <Go to ISI>://WOS:000483195200039